Vibrational investigation and phase transitions in the $KMnF_3$ doped perovskite crystals (Li^+, Na^+, Rb^+ and Cs^+)

2002 J. Phys.: Condens. Matter 14 5433

(http://iopscience.iop.org/0953-8984/14/21/317)

INSTITUTE OF PHYSICS PUBLISHING JOURNAL OF PHYSICS: CONDENSED MATTER

J. Phys.: Condens. Matter **14** (2002) 5433–5448 PII: S0953-8984(02)34643-5

Vibrational investigation and phase transitions in the $KMnF_3$ doped perovskite crystals (Li^+, Na^+, Rb^+ and Cs^+)

J Kapusta[1], **Ph Daniel**[2] **and A Ratuszna**[1]

[1] August Chełkowski Institute of Physics, University of Silesia, Uniwersytecka 4, 40-007 Katowice, Poland
[2] Laboratoire de Physique de l'Etat Condensé, UMR CNRS No 6087, Université du Maine, Avenue O Messiaen, 72085 Le Mans Cedex 9, France

E-mail: jkapusta@us.edu.pl

Received 7 March 2002
Published 16 May 2002
Online at stacks.iop.org/JPhysCM/14/5433

Abstract

The influence of substitution of Li^+, Na^+, Rb^+ and Cs^+ ions in the archetype $KMnF_3$ perovskite crystal was studied by the Raman method. The Raman spectra of $(K_{1-x}A_x)MnF_3$ mixed crystals ($x \leqslant 0.15$) were recorded in the range between 30 and 300 K and interpreted in terms of a 'one-mode' behaviour. Attention was paid to evidence of the static and dynamical disorder. From this point of view the behaviour of hard Raman modes versus temperature has been studied together with two unexpected broad Raman bands in the normally inactive ideal cubic phase. The existence of these two broad peaks in the theoretically inactive cubic phase and also the persistence of the hard Raman modes of the tetragonal phase in cubic symmetry suggest the existence of a large structural disorder far above the cubic-to-tetragonal phase transition. The results of Raman investigations are discussed in the more general framework of structural disorder in perovskite systems.

1. Introduction

Over the past three decades the structure of the $KMnF_3$ perovskite has been extensively investigated, especially because, together with $SrTiO_3$, it represents an archetype compound for phase transitions. By using various experimental techniques, it has been shown that 'pure' $KMnF_3$ undergoes several structural phase transitions (SPTs) related to rotation of MnF_6 octahedra (e.g. [1–7]).

The first transition, from the cubic to tetragonal phase, which is slightly of first-order character, occurs at around $T_{1C} = 186$ K and corresponds to the alternate rotation of the MnF_6 octahedra around fourfold cubic axes ($a^0a^0c^-$ in the Glazer formalism [8]). This transition is associated with a softening of the R'_{15} zone boundary mode located at the $R(1/2, 1/2, 1/2)$

Table 1. Sequences of SPT in mixed $(K_{1-x}A_x)MnF_3$ crystals, where A = Li^+, Na^+, Rb^+ and Cs^+. Comparison with 'pure' $KMnF_3$ [7] is given.

$KMnF_3$					
cubic	$\xrightarrow[T_{1C}]{}$ tetragonal	$\xrightarrow[T_{2C}]{}$ monoclinic			
$a^0a^0a^0$	$a^0a^0c^-$	$a^-b^+a^-$			
$KMnF_3$: Li^+					
cubic	$\xrightarrow[T_{1C}]{}$ tetragonal	$\xrightarrow[T_{2C}]{}$ tetragonal + orthorhombic		$\xrightarrow[T_{3C}]{}$ orthorhombic	
$a^0a^0a^0$	$a^0a^0c^-$	$a^0a^0c^-$	$a^0b^+c^-$	$a^0b^+c^-$	
$KMnF_3$: Na^+					
cubic	$\xrightarrow[T_{1C}]{}$ tetragonal	$\xrightarrow[T_{2C}]{}$ orthorhombic			
$a^0a^0a^0$	$a^0a^0c^-$	$a^0b^+c^-$			
$KMnF_3$: Rb^+					
cubic	$\xrightarrow[T_{1C}]{}$ tetragonal	$\xrightarrow[T_{2C}]{}$ tetragonal + monoclinic		$\xrightarrow[T_{3C}]{}$ monoclinic	
$a^0a^0a^0$	$a^0a^0c^-$	$a^0a^0c^-$	$a^-b^+a^-$	$a^-b^+a^-$	
$KMnF_3$: Cs^+					
cubic	$\xrightarrow[T_{1C}]{}$ tetragonal	$\xrightarrow[T_{2C}]{}$ tetragonal + monoclinic		$\xrightarrow[T_{3C}]{}$ monoclinic	
$a^0a^0a^0$	$a^0a^0c^-$	$a^0a^0c^-$	$a^-b^+a^-$	$a^-b^+a^-$	

point of reciprocal space. It is followed by an additional lower-temperature phase transition, at about $T_{2C} = 80$ K, with a strong first-order character [3, 9] associated with the softening of phonons which have the M_2 symmetry (zone boundary mode located at the $M(1/2, 0, 1/2)$ point of reciprocal space). The structure of the lowest-temperature phase seems to correspond to a monoclinic symmetry with $P2_1/m$ space group and due to the $a^-b^+c^-$ tilt system [7] (the superscript + is used to denote the in-phase octahedron tilting while the − superscript indicates an anti-phase tilt). The existence, in a short temperature range between 80 and 90 K, of an orthorhombic $Bmmb$ symmetry (with $a^0b^+c^-$ tilt system) is still a subject of controversy [9].

It is well known that Raman scattering is able to give valuable information towards better understanding of the mechanism of SPT, especially it appears as a good local probe to interpret the role of impurities in such a mechanism. In the case of $KMnF_3$ it was shown that even small impurities, which might have been introduced during the technology process, provide an important perturbation in the temperatures of the SPT and also contribute to new distortions [10]. Therefore we present here the full Raman analysis of the mixed $K_{1-x}A_xMnF_3$ crystals (A = Li^+, Na^+, Rb^+ and Cs^+) when the admixtures of alkali metals with radii smaller than K^+ ($r_K = 1.64$ Å), such as Li^+ ($r_{Li} = 1.15$ Å) and Na^+ ($r_{Na} = 1.39$ Å), and larger, such as Rb^+ ($r_{Rb} = 1.72$ Å) and Cs^+ ($r_{Cs} = 1.88$ Å), are introduced, in a controlled manner, instead of a K^+ ion. The sequences of SPTs in the mixed crystals studied in comparison with 'pure' $KMnF_3$ are summarized in table 1.

2. Experimental details

Good quality pink crystals of $(K_{1-x}Li_x)MnF_3$ ($x = 0.019$ and 0.043), $(K_{1-x}Na_x)MnF_3$ ($x = 0.029$, 0.048 and 0.065), $(K_{1-x}Rb_x)MnF_3$ ($x = 0.01$ and 0.15) and also $(K_{1-x}Cs_x)MnF_3$ with $x = 0.013$ were grown by the Bridgmann technique [11]. About 1 cm^3 single crystals were cut and orientated by the x-ray Laüe method along fourfold cubic axes. The exact concentration of Na^+, Li^+, Rb^+ and Cs^+ in $KMnF_3$ was checked assuming the Vegard behaviour of the cubic cell parameters.

The Raman spectra were collected on a Dilor Z-24 single-channel triple monochromator coupled with a Coherent 90-3 argon ion laser. The 488 nm excitation line was chosen with

Table 2. Irreducible representations associated with the motions of the three different types of atom in mixed $(K_{1-x}A_x)MnF_3$ compounds (A = Li^+, Na^+, Rb^+ and Cs^+).

Cubic phase—$Pm3m$ (O_h^1)	Tetragonal phase—$I4/mcm$ (D_{4h}^{18})
$a^0a^0a^0$	$a^0a^0c^-$
$\Gamma_K = F_{1u}$	$\Gamma_K = B_{2g} \oplus E_g \oplus A_{2u} \oplus E_u$
$\Gamma_{Mn} = F_{1u}$	$\Gamma_{Mn} = A_{1u} \oplus A_{2u} \oplus 2E_u$
$\Gamma_F = 2F_{1u} \oplus F_{2u}$	$\Gamma_F = A_{1g} \oplus 2A_{2g} \oplus B_{1g} \oplus B_{2g} \oplus 2E_g \oplus 2A_{2u} \oplus B_{1u} \oplus 3E_u$
$\Gamma_{total} = 4F_{1u} \oplus F_{2u}$	$\Gamma_{total} = A_{1g} \oplus 2A_{2g} \oplus B_{1g} \oplus 2B_{2g} \oplus 3E_g \oplus A_{1u} \oplus 4A_{2u} \oplus B_{1u} \oplus 6E_u$
Γ_{Raman}—no Raman lines	$\Gamma_{Raman} = A_{1g} \oplus B_{1g} \oplus 2B_{2g} \oplus 3E_g$ 7 active Raman lines
Low-temperature phase	
Orthorhombic phase—$Pnma$ (D_{2h}^{16})	Monoclinic phase—$P2_1/m$ (C_{2h}^2)
$a^0b^+c^-$	$a^-b^+a^-$
$\Gamma_K = 2A_g \oplus B_{1g} \oplus 2B_{2g} \oplus B_{3g} \oplus A_u \oplus 2B_{1u} \oplus B_{2u} \oplus 2B_{3u}$	$\Gamma_K = 4A_g \oplus 2B_g \oplus 2A_u \oplus 4B_u$
$\Gamma_{Mn} = 3A_u \oplus 3B_{1u} \oplus 3B2_u \oplus 3B_{3u}$	$\Gamma_{Mn} = 6A_u \oplus 6B_u$
$\Gamma_F = 5A_g \oplus 4B_{1g} \oplus 5B_{2g} \oplus 4B_{3g} \oplus 4A_u \oplus 5B_{1u} \oplus 4B_{2u} \oplus 5B_{3u}$	$\Gamma_F = 10A_g \oplus 8B_g \oplus 8A_u \oplus 10B_u$
$\Gamma_{total} = 7A_g \oplus 5B_{1g} \oplus 7B_{2g} \oplus 5B_{3g} \oplus \updownarrow\rightarrow 8A_u \oplus 10B_{1u} \oplus 8B_{2u} \oplus 10B_{3u}$	$\Gamma_{total} = 14A_g \oplus 10B_g \oplus 16A_u \oplus 20B_u$
$\Gamma_{Raman} = 7A_g \oplus 5B_{1g} \oplus 7B_{2g} \oplus 5B_{3g}$ 24 Raman lines	$\Gamma_{Raman} = 14A_g \oplus 10B_g$ 24 Raman lines

an incident power not exceeding 500 mW. Low-temperature measurements were performed in the temperature range from 30 up to 300 K with the help of a Leybold cryogenerator.

3. Results and discussion

The analysis of the symmetries of the vibrational normal modes was made on the basis of the site symmetry method as described by Rousseau *et al* [12]. The number and the symmetry of the Raman-active modes were obtained for each tilt system which occurs in these mixed crystals. The results of these group theory calculations are summarized in table 2. No Raman mode is active in the cubic phase, while the cubic-to-tetragonal phase transition should be characterized in the Raman spectra by the appearance of seven Raman modes. Additionally, the transition from the tetragonal to orthorhombic (or monoclinic) phase is expected to be clearly noticed by Raman spectroscopy, because seven modes are active in the tetragonal phase whereas 24 are predicted in the low-temperature phase. Since the number of expected active Raman modes in the orthorhombic and monoclinic symmetries is the same, it appears that the Raman technique is not the best method to distinguish these two symmetries, also because these two different distortions are very close to each other and originate from the same tetragonal phase.

Attention was paid to the evolution of frequencies of active Raman lines versus concentration of dopants, and generally two behaviours can be evidenced by Raman scattering. In the case of the first, named the 'one-mode' group, the frequencies of the vibrational modes change continuously and approximately linearly with concentration from one end member to the other one of the phase diagram. Moreover the strength of the modes remains approximately constant [13, 14]. In the 'two-mode' group, the two distinct allowed optic modes are observed to occur at separate frequencies close to those of the 'pure' crystals.

Figures 1(*a*)–(*c*) show the evolution of frequencies of the main Raman peaks with concentration of dopants for $(K_{1-x}Li_x)MnF_3$, $(K_{1-x}Na_x)MnF_3$ and $(K_{1-x}Rb_x)MnF_3$ mixed systems, respectively. It can be clearly seen that the main Raman peaks shift linearly with concentration; this means that all the mixed systems studied belong to the 'one-mode' group, which can be physically interpreted as the mixing of two comparable and similar structures.

Such a behaviour is also clearly seen in figure 2, which shows the recorded Raman spectra of the mixed crystals $(K_{1-x}Li_x)MnF_3$ ($x = 0$, 0.019 and 0.043), $(K_{1-x}Na_x)MnF_3$ ($x = 0$, 0.029, 0.048, 0.065 and 0.14) and $(K_{1-x}Cs_x)MnF_3$ ($x = 0$ and 0.013) in their low-temperature phases at $T = 30$ K, and also $(K_{1-x}Rb_x)MnF_3$ ($x = 0$, 0.01 and 0.15) in the tetragonal phase at $T = 150$ K (since $K_{0.85}Rb_{0.15}MnF_3$ is tetragonal at 30 K, while $K_{0.99}Rb_{0.01}MnF_3$ is monoclinic at the same temperature).

'One-mode' behaviour suggests that all Raman spectra of the $(K_{1-x}A_x)MnF_3$ mixed crystals could be interpreted based on a knowledge of the spectra of the pure crystal, in this case the typical $KMnF_3$ compound [4, 7, 15]. The results of the proposed assignment are summarized in tables 3–6. In the case of $(K_{1-x}Na_x)MnF_3$ compounds, the assignment was suggested considering also the previous results of 'pure' $NaMnF_3$ crystals [16].

The positions of the Raman lines were precisely determined using a standard fitting procedure and assuming a Gaussian shape of the Raman lines. Considering the low-temperature phases (monoclinic or orthorhombic), the number of active Raman modes depends on the kind and number of dopants. In the case of the Na^+-doped sample a smaller number of Raman peaks was detected for $(K_{1-x}Na_x)MnF_3$ crystals (see table 3(a)). Additionally, the full width at half maximum (FWHM) increases when the crystals are richer in Na^+ due to the probable growing structural disorder [20]. In the $K_{0.86}Na_{0.14}MnF_3$ crystal the usual splitting of the orthorhombic lines originating from tetragonal peaks could not be observed because of the significant broadening of lines (up to 60 cm^{-1}) [21]. About the same number of Raman lines—13 (in comparison with 14 which were observed for 'pure' $KMnF_3$) was detected in the Raman spectra of $K_{0.99}Rb_{0.01}MnF_3$ and $K_{0.987}Cs_{0.013}MnF_3$ crystals (see tables 5 and 6). However, a reverse situation is noticed for the Li^+-doped compounds. Actually two additional lines are probably observed compared with 'pure' $KMnF_3$. This experimental evidence can be connected to the very small radius of Li^+, compared with K^+, which allows an easier rotation of octahedra and then allows active zone boundary cubic modes in the low-temperature phase.

The temperature evolution of the Raman spectra and changes of the Raman shifts versus temperature for $K_{0.99}Rb_{0.01}MnF_3$, as an example, are presented in figures 3 and 4. The two SPTs were observed: the first, at T_{1C}, from cubic to tetragonal symmetry and the second, at T_{2C}, from tetragonal to low-temperature symmetry. The symmetry of the low-temperature phase depends on the kind of dopant and it is either orthorhombic or monoclinic (see table 1). Similarly to 'pure' $KMnF_3$ [7], the upper phase transition, at T_{1C}, is due to softening of the triply degenerate R'_{15} cubic mode at the $R(0.5, 0.5, 0.5)$ point of the cubic Brillouin zone. This soft mode corresponds to antiphase rotations of the MnF_6 octahedra around the cubic [001] axis ($a^0a^0c^-$ in Glazer classification [8]). The low-temperature phase transition, at T_{2C}, is characterized by abrupt changes in the Raman spectra. As evidenced by figures 3 and 4, the appearance of several low-frequency modes (together with temperature decrease) below T_{2C} is noticed. These modes (with A_g symmetries) have smaller line width FWHM than the other lines detected in spectra of the crystals studied (about 6 cm^{-1} compared with 10 cm^{-1}). Such a behaviour of these several modes originating from the R'_{15}, M_2 and X_5 zone boundary cubic modes (see tables 4–6) shows the first-order character of this low-temperature phase transition [19]. Similar behaviour is observed for $KMnF_3$ doped by Li^+ and Cs^+. This means that the substitution of larger ions such as Rb^+ and Cs^+ and also smaller ones such as Li^+ instead of the K^+ ions does not change the character of the tetragonal to monoclinic or tetragonal to

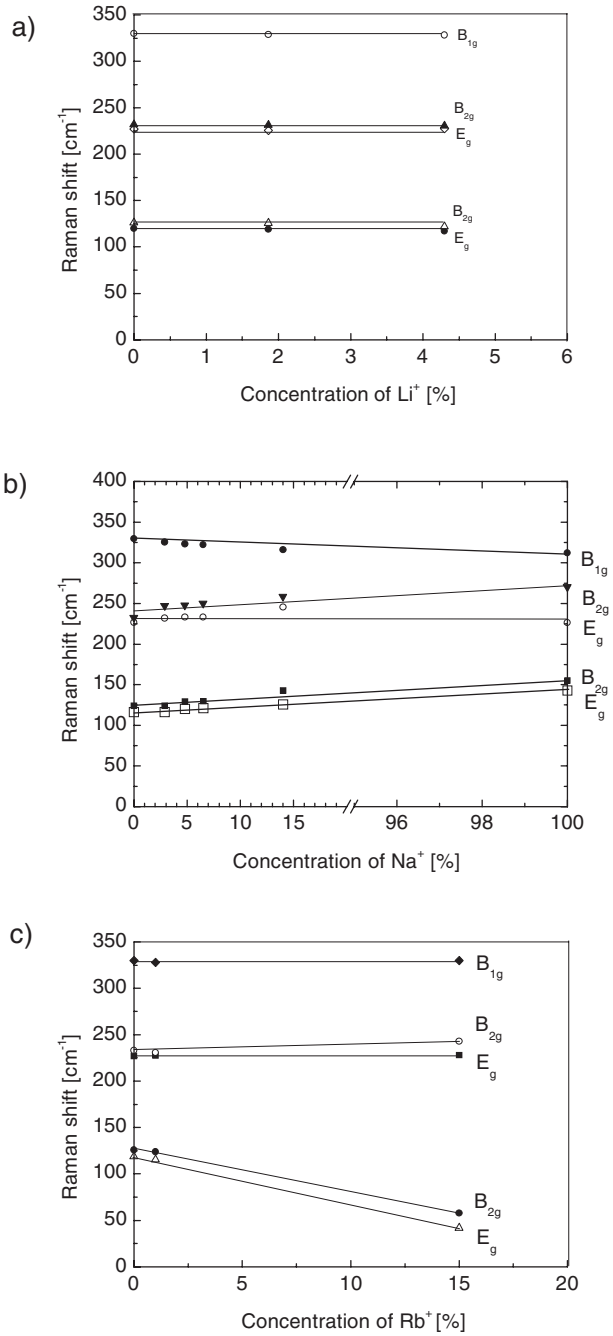

Figure 1. Evolution of the Raman shift of tetragonal lines versus concentration of (*a*) Li^+ in the mixed $K_{1-x}Li_xMnF_3$ crystals ($x = 0.019$ and 0.043), (*b*) Na^+ in the mixed $K_{1-x}Na_xMnF_3$ compounds ($x = 0.029$, 0.048 and 0.065) and (*c*) Rb^+ in the mixed $K_{1-x}Rb_xMnF_3$ crystals ($x = 0.01$ and 0.15).

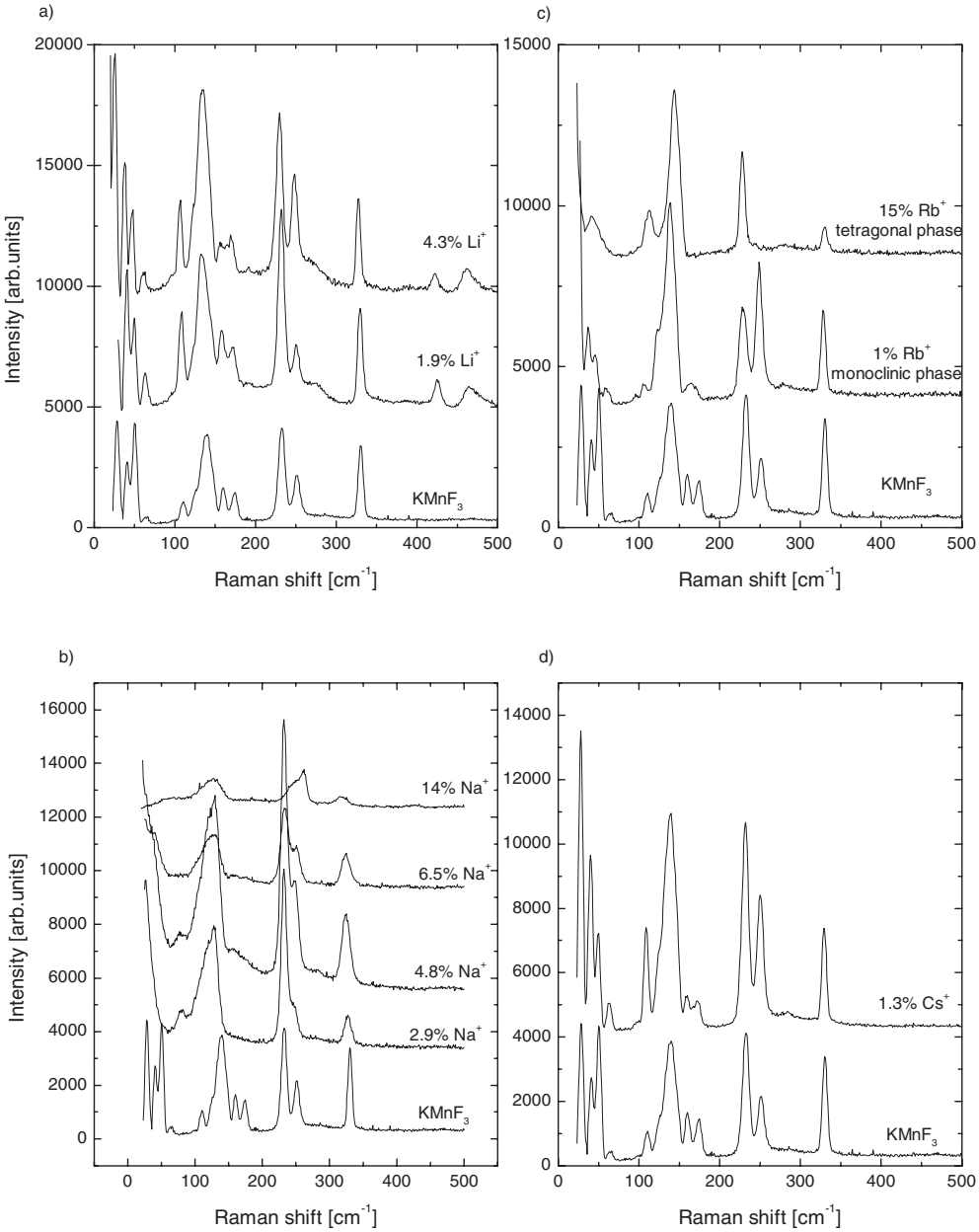

Figure 2. Experimental Raman spectra of (*a*) the mixed $K_{1-x}Li_xMnF_3$ crystals ($x = 0.0$, 0.019 and 0.043) at $T = 30$ K, (*b*) the mixed $K_{1-x}Na_xMnF_3$ compounds ($x = 0.0$, 0.029, 0.048, 0.065 and 0.14) at $T = 30$ K, (*c*) the mixed $K_{1-x}Rb_xMnF_3$ crystals ($x = 0.0$, 0.01 and 0.15) in the tetragonal phase at $T = 150$ K and (*d*) the mixed $K_{1-x}Cs_xMnF_3$ ($x = 0.0$, 0.013) at $T = 30$ K.

orthorhombic phase transition, which seems to possess the first-order character. Different behaviour is observed in case of the $(K_{1-x}Na_x)MnF_3$ mixed systems ($x = 0.029$, 0.048 and 0.065) where the sharp, low-frequency lines are not observed [21], which seems to evidence that the mechanism of this SPT is strongly affected by this dopant.

Table 3. (a). Assignment of Raman modes of the $(K_{1-x}Na_x)MnF_3$ mixed crystals ($x = 0.029$, 0.048 and 0.065) in the low-temperature phase at $T \approx T_{2C} - 40$ K and in the tetragonal phase at $T \approx T_{2C} + 50$ K. Comparison with the assignment of 'pure' $KMnF_3$ [7] and 'pure' $NaMnF_3$ [16] is given. Symbols $\updownarrow$ or $\updownarrow\!\!\!\!\rightarrow$ indicate the impossibility of differentiating unambiguously the assignment of a Raman mode between two or three eigensymmetries, respectively, generally originating from the same cubic mode. (s) is used to designate a soft mode.

Orthorhombic (1) and monoclinic (2) labelling (cm^{-1}) (1)	(2)	$KMnF_3$ $T = 50$ K (cm^{-1})	2.9% Na $T = 70$ K (cm^{-1})	4.8% Na $T = 70$ K (cm^{-1})	6.5% Na $T = 60$ K (cm^{-1})	$NaMnF_3$ $T = 40$ K (cm^{-1})
B_{1g}	B_g	27.9	25.0	21.0	24.0	n.o.
B_{2g}	A_g	40.1	36.8	33.9	39.7	n.o.
A_g	A_g	96.0	79.0	79.0	80.0	183.0
A_g	A_g	49.6	n.o.	n.o.	n.o.	250.0
A_g	A_g	64.7	n.o.	n.o.	n.o.	88.0
B_{2g}	A_g	n.o.	n.o.	n.o.	n.o.	140.0
A_g	A_g	110.8	102.0	102.0	103.9	143.0
B_{3g}	B_g	124.4	115.1	115.9	118.0	96.0
B_{2g}	A_g	135.1	130.0	129.7	130.9	155.0
B_{1g}	B_g	n.o.	n.o.	n.o.	n.o.	182.0
B_{1g}	B_g	n.o.	n.o.	n.o.	n.o.	160.0
B_{3g}	B_g	160.0	158.2	160.0	158.0	n.o.
A_g	A_g	172.2	n.o.	n.o.	178.0	212.0
B_{2g}	A_g	n.o.	n.o.	n.o.	n.o.	201.0
B_{2g}	A_g	n.o.	n.o.	n.o.	n.o.	n.o.
B_{3g}	B_g	231.4	232.0	232.4	233.5	226.0
A_g	A_g	251.2	246.0	248.0	250.8	270.0
B_{2g}	A_g	n.o.	n.o.	n.o.	n.o.	293.0
B_{1g}	B_g	329.7	327.0	324.6	324.3	312.0
B_{3g}	B_g	n.o.	n.o.	n.o.	n.o.	302.0
A_g	A_g	n.o.	n.o.	n.o.	n.o.	319.0
B_{1g}	B_g	n.o.	n.o.	n.o.	n.o.	426.0
B_{2g}	A_g	n.o.	n.o.	n.o.	n.o.	n.o.
B_{3g}	B_g	n.o.	n.o.	n.o.	n.o.	n.o.

Figure 5 shows the evolution of experimental Raman spectra versus temperature in the cubic phase for the $K_{0.957}Li_{0.043}MnF_3$ crystal. It can be noticed that in the cubic phase, where no Raman line is predicted by group theory, two broad bands located at about 210 and 280 cm^{-1} are observed. Moreover, as shown in figure 5, these two broad bands have already appeared in the tetragonal phase 'under' the tetragonal peaks. These unusual cubic lines were still detected in 'pure' $KMnF_3$ [4,7,18] but are also evidenced for all dopants, i.e. Na^+, Li^+, Rb^+ and Cs^+. The value of the FWHM of these bands is about 50–60 cm^{-1}, and it is large compared with typical values of 10 cm^{-1} that the tetragonal Raman modes have. For the $K_{0.957}Li_{0.043}MnF_3$ crystal, high-temperature experiments in a temperature range from 300 to 673 K were performed with the aim of studying the temperature behaviour of the unusual cubic bands. The changes of Raman frequencies of these broad bands in the cubic phase versus temperature are shown in figure 6. It can be noticed that the mode located at 209 cm^{-1} (at 300 K) decreases slightly in frequency up to 203 cm^{-1}(at 673 K), while the second mode, located at 280.5 cm^{-1} (at 300 K), increases in frequency up to 305 cm^{-1} (at 673 K) together with temperature increase.

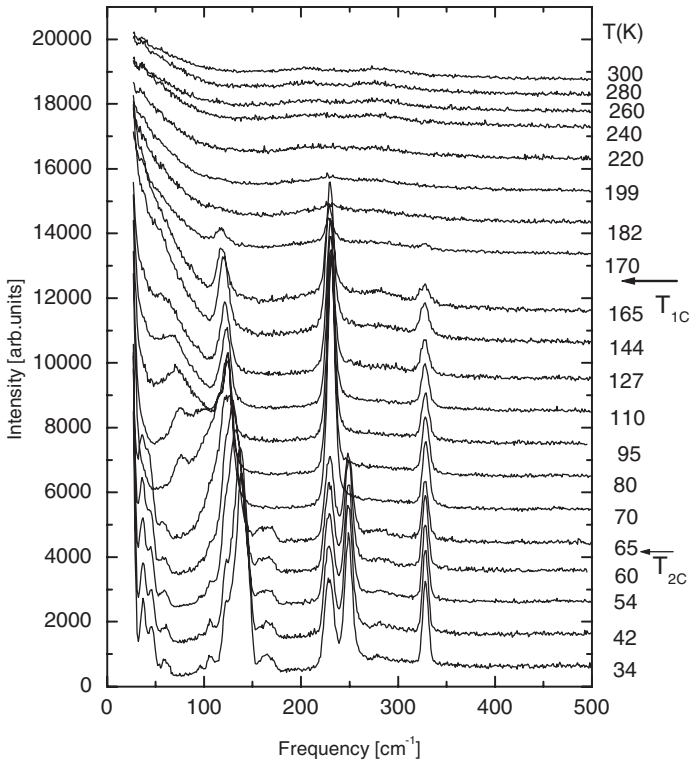

Figure 3. Evolution of the experimental Raman spectra versus temperature for the $K_{0.99}Rb_{0.01}MnF_3$ crystal.

Table 3. (b). Assignment of Raman modes of the $(K_{1-x}Na_x)MnF_3$ mixed crystals ($x = 0.029$, 0.048 and 0.065) in tetragonal phase at $T \approx T_{2C} + 50$ K. Comparison with the assignment of 'pure' $KMnF_3$ [7] and $K_{0.86}Na_{0.14}MnF_3$ [21] is given. (s) is used to designate a soft mode.

Cubic modes	Tetragonal modes	$KMnF_3$ $T = 140$ K (cm^{-1})	2.9% of Na $T = 160$ K (cm^{-1})	4.8% of Na $T = 148$ K (cm^{-1})	6.5% of Na $T = 140$ K (cm^{-1})	14% of Na $T = 83$ K (cm^{-1})
R'_{15}	E_g	n.o.	n.o.	n.o.	n.o.	n.o.
	A_{1g}	61.7(s)	62.2	67.5	70.0	74.3
R'_{25}	E_g	116.0	116.5	120.0	121.5	125.6
	B_{2g}	124.0	124.3	129.0	130.0	183.0
R'_{25}	E_g	227.0	231.9	233.0	233.2	245.3
	B_{2g}	232.4	247.0	247.7	249.7	258.3
R_{12}	B_{1g}	329.5	325.5	323.0	322.0	315.8

The large value of FWHM seems to indicate that the origin of these broad bands could be related to the existence of structural disorder. Moreover, the origin of these bands seems to be similar to those in 'pure' $KMnF_3$ [7]. The band located at about 210 cm^{-1} is related to the R'_{25}–M_3 phonon branch, while the band located at about 280 cm^{-1} is involved in the R'_{15}–M_2 phonon branch combined with the R'_{25}–M_4 and R'_{25}–M'_5 phonon branches, where

Table 4. Assignment of Raman modes of the $(K_{1-x}Li_x)MnF_3$ mixed crystals ($x = 0.019$ and 0.043) in tetragonal phase (at $T \approx T_{1C} - 40$ K) and in the low-temperature phases (at $T \approx T_{2C} - 60$ K). Comparison with the assignment of 'pure' $KMnF_3$ [7] is given. Symbols $\updownarrow$ or $\updownarrow\!\!\rightarrow$ indicate the impossibility of differentiating unambiguously the assignment of a Raman mode between two or three eigensymmetries, respectively. (s) is used to designate a soft mode.

Cubic modes	Tetragonal modes	$KMnF_3$ $T =$ 150 K (cm^{-1})	1.9% of Li^+ $T =$ 160 K (cm^{-1})	4.3% of Li^+ $T =$ 160 K (cm^{-1})	Orthorhombic (1) and monoclinic (2) labelling (1)	(2)	$KMnF_3$ $T =$ 30 K (cm^{-1})	1.9% of Li^+ $T =$ 50 K (cm^{-1})	4.3% of Li^+ $T =$ 46 K (cm^{-1})
	E_g	n.o.	n.o.	n.o.	B_{1g}	B_g	28.5	n.o.	25.8
R'_{15}					B_2	A_g	40.9	40.6	37.4
	A_{1g}	61.2(s)	59.5(s)	58.3(s)	A_g	A_g	98.3	97.8	95.4
M_2	X_4	i	i	i	A_g	A_g	50.4	49.8	47.1
X_5	X_4	i	i	i	A_g	A_g	64.6	53.4	60.1
	X_3	i	i	i	B_{2g}	A_g	n.o.	n.o.	n.o.
	E_g	120.3	118.8	117.0	A_g	A_g	110.4	108.8	106.2
R'_{25}					B_{3g}	B_g	123.5	120.0	120.1
	B_{2g}	126.2	125.7	122.0	B_{2g}	A_g	139.2	133.1	132.4
X_1	X_1	i	i	i	B_{1g}	B_g	n.o.	144.2 ?	143.0 ?
M_5	X_1	i	i	i	B_{1g}	B_g	n.o.	n.o.	n.o.
	X_2	i	i	i	B_{3g}	B_g	160.4	158.7	156.2
X_5	X_4	i	i	i	A_g	A_g	173.7	171.8	168.0
	X_3	i	i	i	B_{2g}	A_g	187.5	n.o.	n.o.
	E_g	227.0	225.6	227.5	B_{2g}	A_g	n.o.	n.o.	n.o.
R'_{25}					B_{3g}	B_g	251.3	250.0	248.2
	B_{2g}	232.0	232.3	230.7	A_g	A_g	232.5	232.0	229.8
M_4	X_4	i	i	i	B_{2g}	A_g	n.o.	n.o.	n.o.
R_{12}	B_{1g}	330.0	329.8	328.2	B_{1g}	B_g	330.3	329.7	327.5
	A_{2g}	i	i	i	B_{3g}	B_g	n.o.	n.o.	n.o.
M_3	X_3	i	i	i	A_g	A_g	n.o.	n.o.	n.o.
X_1	X_1	i	i	i	B_{1g}	B_g	n.o.	425.1 ?	420.8 ?
M_1	X_3	i	i	i	B_{2g}	A_g	n.o.	n.o.	n.o.
R_1	A_{2g}	i	i	i	B_{3g}	B_g	n.o.	n.o.	n.o.

R'_{15} designates the soft cubic mode responsible for the phase transition. The involvement of the R'_{15} soft mode is demonstrated by the frequency increase with temperature of the band concerned. Particular attention can be paid to modes which are not directly involved in the transition mechanism. These temperature-independent modes are named 'hard modes' and are generally well resolved, so their intensity and linewidth evolution versus temperature can be established. Figure 7 shows a typical example of temperature evolution of the FWHM and Raman intensities for the $K_{0.99}Rb_{0.01}MnF_3$ crystal (as an example). We focused on the two high-frequency hard Raman modes of tetragonal symmetries B_{2g} and B_{1g} originating from R'_{25} and R_{12} cubic modes and located at about 230 and 330 cm^{-1}, respectively. All these modes can be observed from the lowest temperatures up to T_{1C} (temperature of cubic to tetragonal SPT). It is clearly seen in figure 7 that the hard Raman modes studied are a good probe to evidence the symmetry changes. This is illustrated by significant drops (close to the T_{1C} and T_{2C}) in their strength and their FWHM. Such a behaviour has been also reported by Di Antonio *et al* [17] in the mixed perovskite ferroelectrics ($KTa_{1-x}Nb_xO_3$ and $K_{1-x}Li_xTaO_3$), by Bruce *et al* [18] in

Table 5. Assignment of Raman modes of the $K_{0.99}Rb_{0.01}MnF_3$ and $K_{0.85}Rb_{0.15}MnF_3$ crystals in the low-temperature (at $T \approx T_{2C} - 30$ K) and tetragonal (at $T \approx T_{1C} - 60$ K) phases. Comparison with the assignment of 'pure' $KMnF_3$ [7] is given. (s) is used to designate a soft mode. Symbols $\updownarrow$ or $\updownarrow\!\!\!\!\rightarrow$ indicates the impossibility of differentiating unambiguously the assignment of a Raman mode between two or three eigensymmetries, respectively.

Cubic modes	Tetragonal modes	$KMnF_3$ $T = 125$ K (cm^{-1})	1% of Rb^+ $T = 110$ K (cm^{-1})	15% of Rb^+ $T = 30$ K (cm^{-1})	Orthorhombic (1) and monoclinic (2) labelling (1)	(2)		$KMnF_3$ $T = 60$ K (cm^{-1})		1.0% of Rb^+ $T = 30$ K (cm^{-1})
	E_g	n.o.	n.o.	113.0	B_{1g}	B_g		28.5		27.0
R'_{15}					B_2	A_g		40.9		37.1
	A_{1g}	74.5	67.5	144.0	A_g	A_g		98.3		95.8
M_2	X_4	i	i	i	A_g	A_g		50.4		49.5
X_5	X_4	i	i	i	A_g	A_g	$\updownarrow$	64.6	$\updownarrow$	59.8
	X_3	i	i	i	B_{2g}	A_g		n.o.		n.o.
	E_g	118.9	115.6	42.0	A_g	A_g		110.4		106.9
R'_{25}					B_{3g}	B_g	$\updownarrow\!\!\!\!\rightarrow$	123.5	$\updownarrow\!\!\!\!\rightarrow$	124.6
	B_{2g}	125.7	123.7	58.0	B_{2g}	A_g		139.2		138.7
X_1	X_1	i	i	i	B_{1g}	B_g		n.o.		n.o.
M_5	X_1	i	i	i	B_{1g}	B_g	$\updownarrow$	n.o.	$\updownarrow$	n.o.
	X_2	i	i	i	B_{3g}	B_g		160.4		160.7
X_5	X_4	i	i	i	A_g	A_g	$\updownarrow$	173.7	$\updownarrow$	170.2
	X_3	i	i	i	B_{2g}	A_g		187.5		n.o.
	E_g	227.0	227.0	228.0	B_{2g}	A_g		n.o.		n.o.
R'_{25}					B_{3g}	B_g	$\updownarrow\!\!\!\!\rightarrow$	251.3	$\updownarrow\!\!\!\!\rightarrow$	248.9
	B_{2g}	232.8	230.7	243.0	A_g	A_g		232.5		229.2
M_4	X_4	i	i	i	B_{2g}	A_g		n.o.		n.o.
R_{12}	B_{1g}	329.6	328.0	330.0	B_{1g}	B_g	$\updownarrow$	330.3	$\updownarrow$	328.4
	A_{2g}	i	i	i	B_{3g}	B_g		n.o.		n.o.
M_3	X_3	i	i	i	A_g	A_g		n.o.		n.o.
X_1	X_1	i	i	i	B_{1g}	B_g		n.o.		n.o.
M_1	X_3	i	i	i	B_{2g}	A_g		n.o.		n.o.
R_1	A_{2g}	i	i	i	B_{3g}	B_g		n.o.		n.o.

$KMnF_3$ and by Daniel *et al* [19] in $RbCaF_3$. It can also be noticed that this behaviour is much weaker in the case of the $(K_{1-x}Na_x)MnF_3$ mixed crystals [20]. It seems to be associated with the fact that these crystals show very slight distortion, weaker than observed in 'pure' $KMnF_3$ doped by the other dopants i.e. Li^+, Rb^+ and Cs^+ [10]. The intensities of hard Raman modes contain very useful information on the mechanism of SPT. From the expression of the Raman intensity versus polarizability and as stated by Daniel *et al* [19], the intensities of these modes can be expressed as follows:

$$I \propto t^{2\beta}$$

where β is the critical exponent from the order parameter, while $t = (T_{1C} - T)/T_{1C}$ is the reduced temperature. This means that the plot of $\ln(I)$ as a function of $\ln(t)$ should be a straight line with a slope of 2β, which allows to give a value for β. Figure 8 shows such a plot for $K_{0.987}Cs_{0.013}MnF_3$, as an example. The critical exponents deduced from the plot of $\ln(I)$ versus $\ln(t)$ for the $(K_{1-x}A_x)MnF_3$ mixed crystals are listed in table 7. It is clear that for different amounts of the same kind of dopant, the values of β parameter are almost the same. These

Table 6. Assignment of Raman modes of the $K_{0.987}Cs_{0.013}MnF_3$ crystal in both the low-temperature (at $T \approx T_{2C} - 40$ K) and tetragonal (at $T \approx T_{1C} - 40$ K) symmetries. Comparison with the assignment of 'pure' $KMnF_3$ [7] is given. (s) is used to designate a soft mode. Symbols $\updownarrow$ or $\updownarrow\!\!\!\rightarrow$ indicate the impossibility of differentiating unambiguously the assignment of a Raman mode between two or three eigensymmetries, respectively.

Cubic modes	Tetragonal modes	$KMnF_3$ $T = 150$ K (cm^{-1})	1.3% Cs^+ $T = 140$ K (cm^{-1}) [22]	Orthorhombic (1) and monoclinic (2) labelling (1)	(2)		$KMnF_3$ $T = 50$ K (cm^{-1})		1.3% of Cs^+ $T = 30$ K (cm^{-1}) [22]
	E_g	n.o.	n.o.	B_{1g}	B_g		28.5		26.6
R'_{15}				B_2	A_g		40.9		38.8
	A_{1g}	61.2	59.0	A_g	A_g		98.3		100.0
M_2	X_4	i	i	A_g	A_g		50.4		47.9
X_5	X_4	i	i	A_g	A_g	$\updownarrow$	64.6	$\updownarrow$	62.2
	X_3	i	i	B_{2g}	A_g		n.o.		n.o.
	E_g	120.3	118.0	A_g	A_g		110.4		108.0
R'_{25}				B_{3g}	B_g	$\updownarrow\!\!\!\rightarrow$	123.5	$\updownarrow\!\!\!\rightarrow$	125.0
	B_{2g}	126.2	125.0	B_{2g}	A_g		139.2		139.7
X_1	X_1	i	i	B_{1g}	B_g		n.o.		n.o.
M_5	X_1	i	i	B_{1g}	B_g	$\updownarrow$	n.o.	$\updownarrow$	n.o.
	X_2	i	i	B_{3g}	B_g		160.4		159.9
X_5	X_4	i	i	A_g	A_g	$\updownarrow$	173.7	$\updownarrow$	171.7
	X_3	i	i	B_{2g}	A_g		187.5		n.o.
	E_g	227.0	226.4	B_{2g}	A_g		n.o.		n.o.
R'_{25}				B_{3g}	B_g	$\updownarrow\!\!\!\rightarrow$	251.3	$\updownarrow\!\!\!\rightarrow$	250.8
	B_{2g}	232.0	231.8	A_g	A_g		232.5		232.5
M_4	X_4	i	i	B_{2g}	A_g		n.o.		n.o.
R_{12}	B_{1g}	330.0	328.5	B_{1g}	B_g	$\updownarrow$	330.3	$\updownarrow$	329.4
	A_{2g}	i	i	B_{3g}	B_g		n.o.		n.o.
M_3	X_3	i	I	A_g	A_g		n.o.		n.o.
X_1	X_1	i	I	B_{1g}	B_g		n.o.		n.o.
M_1	X_3	i	I	B_{2g}	A_g		n.o.		n.o.
R_1	A_{2g}	i	I	B_{3g}	B_g		n.o.		n.o.

results indicate that the cubic-to-tetragonal phase transition depends on the kind of dopant and not on its amount. This is consistent with the results from x-ray studies [10]. The value of the critical exponent is consistent with the experimental values given in the literature [23] and is close to an Ising three-dimensional model ($\beta = 0.31$).

4. Conclusions

The Raman investigation of the vibrational behaviour of the mixed $K_{1-x}A_xMnF_3$ compounds (where A = Li^+, Na^+, Rb^+ and Cs^+) suggests the existence of a large structural disorder, even in the cubic phase. The existence of this large structural disorder far above the cubic-to-tetragonal transition, at T_{1C}, is noticed from two experimental indications:

- the existence of two broad bands in the theoretically inactive ideal cubic phase
- the persistence of hard Raman modes of the tetragonal phase in the cubic symmetry.

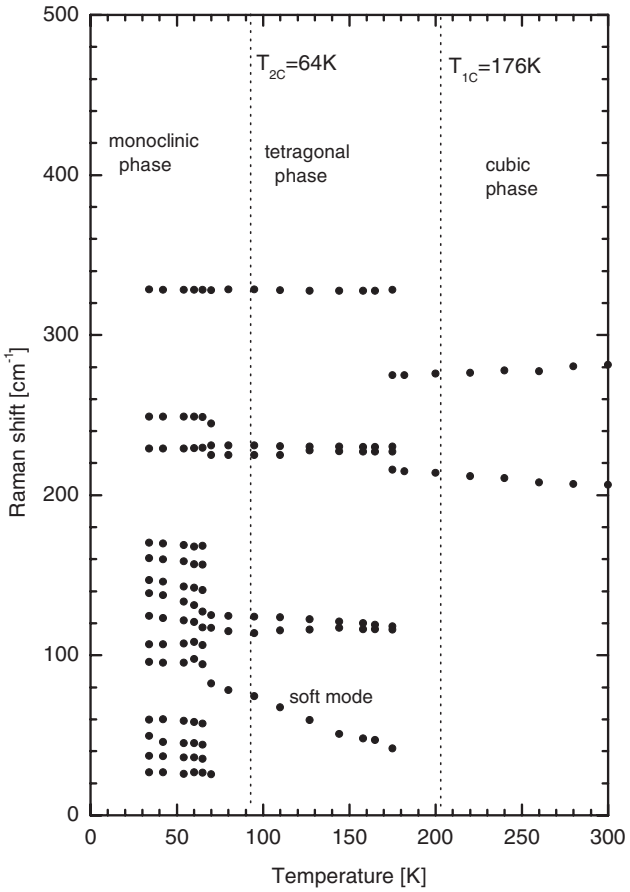

Figure 4. Temperature evolution of Raman shifts for the $K_{0.99}Rb_{0.01}MnF_3$ crystal.

Table 7. The estimated values of β for the mixed $(K_{1-x}A_x)MnF_3$ compounds, where A = Li^+, Na^+, Rb^+ and Cs^+.

Compounds	Order parameters β
$KMnF_3$	0.30(2)
$K_{0.981}Li_{0.019}MnF_3$	0.29(6)
$K_{0.957}Li_{0.043}MnF_3$	0.28(3)
$K_{0.971}Na_{0.029}MnF_3$	0.27(3)
$K_{0.952}Na_{0.048}MnF_3$	0.27(3)
$K_{0.935}Na_{0.065}MnF_3$	0.26(4)
$K_{0.99}Rb_{0.01}MnF_3$	0.23(4)
$K_{0.85}Rb_{0.15}MnF_3$	0.24(3)
$K_{0.987}Cs_{0.013}MnF_3$	0.20(2)

The first feature is noticeable not only for 'pure' $KMnF_3$ but also for all dopants, i.e. Na^+, Li^+, Rb^+ and Cs^+. The persistence of modes from the other symmetries is significant in the case of crystals which are rich in Na^+. For example, in the case of the $K_{0.935}Na_{0.065}MnF_3$ crystal the typical modes of the orthorhombic phase persist in the tetragonal phase up to 140 K (the low-temperature transition occurs at 97 K). Similarly, several tetragonal lines are observed far

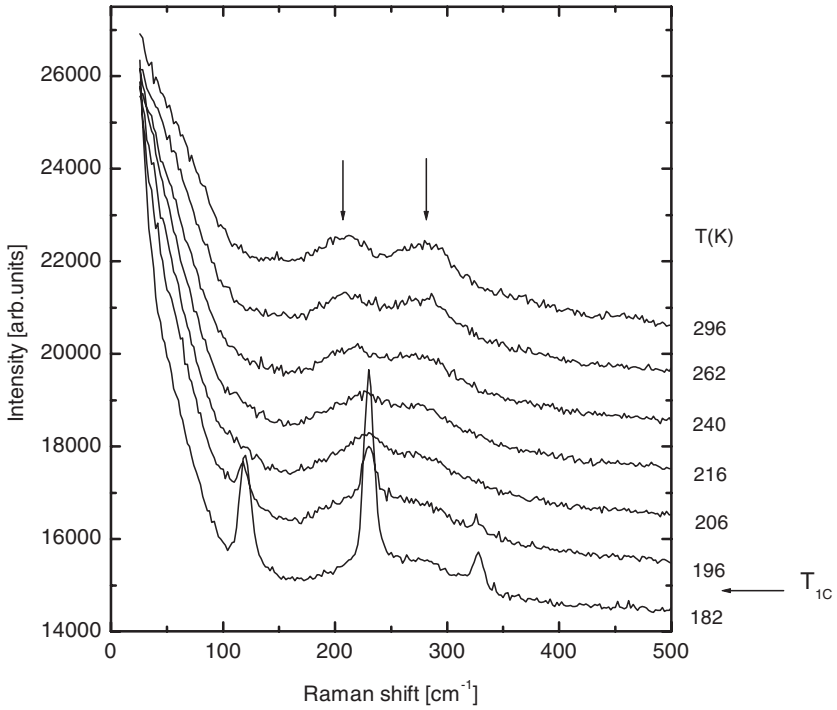

Figure 5. Detailed evolution of the $K_{0.957}Li_{0.043}MnF_3$ Raman spectra versus temperature in the cubic phase.

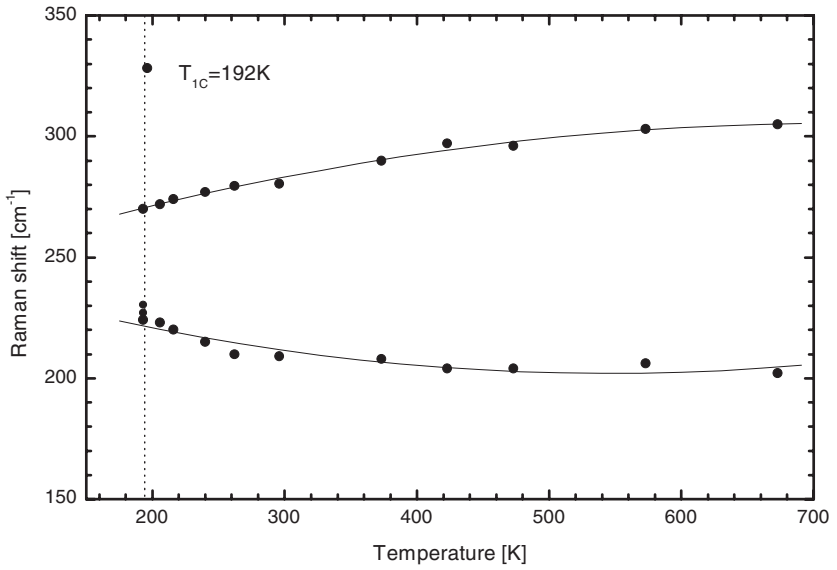

Figure 6. Temperature evolution of Raman frequencies of two broad bands in the cubic phase for the $K_{0.957}Li_{0.043}MnF_3$ crystal. The solid lines are only guides for the eyes.

above (about 40 K) the transition to the cubic phase where no Raman lines are expected by symmetry.

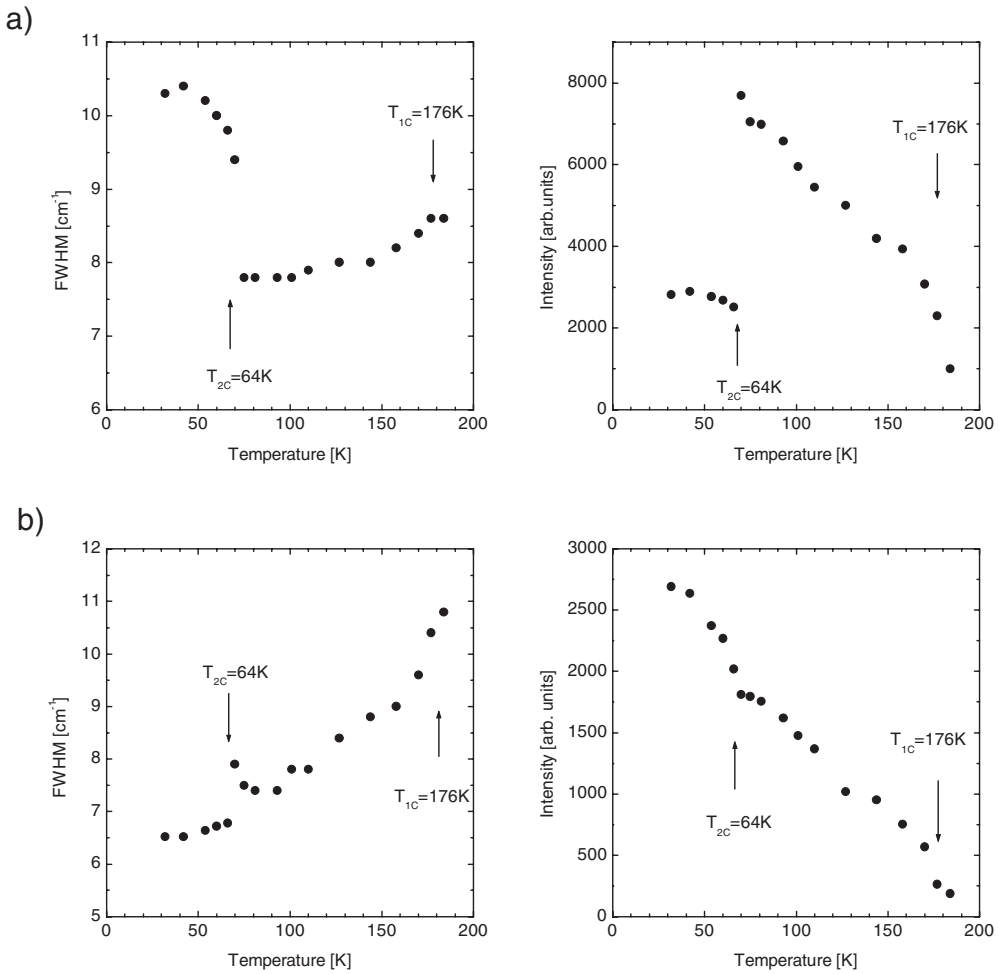

Figure 7. The changes of FWHM and Raman intensities for two hard Raman modes of the $K_{0.99}Rb_{0.01}MnF_3$ crystal: (*a*) mode located at 232.5 cm^{-1} at 30 K (B_{2g} tetragonal symmetry); (*b*) mode located at 330.3 cm^{-1} at 30 K (B_{1g} tetragonal symmetry).

It should be underlined that introduction of a small concentration of Na^+ induces a considerable increase in dynamical disorder, much more strongly than in the case of the other dopants, i.e. Li^+, Rb^+ and Cs^+.

By contrast, the x-ray results give evidence of the usual sequence of SPTs, classically described for the 'pure' $KMnF_3$ compound, with only slight differences. The fact that the diffraction studies do not evidence any disorder in the cubic phase means that the average symmetry is cubic but could be described as the arrangement of disorientated clusters, with a probable nanometric dimension, of which the final arrangement gives rises to the ideal perovskite symmetry. The evidence of these clusters, if they exist, could be found for instance by the EXAFS technique as shown by Yacoby and Stern [24] in oxide perovskites.

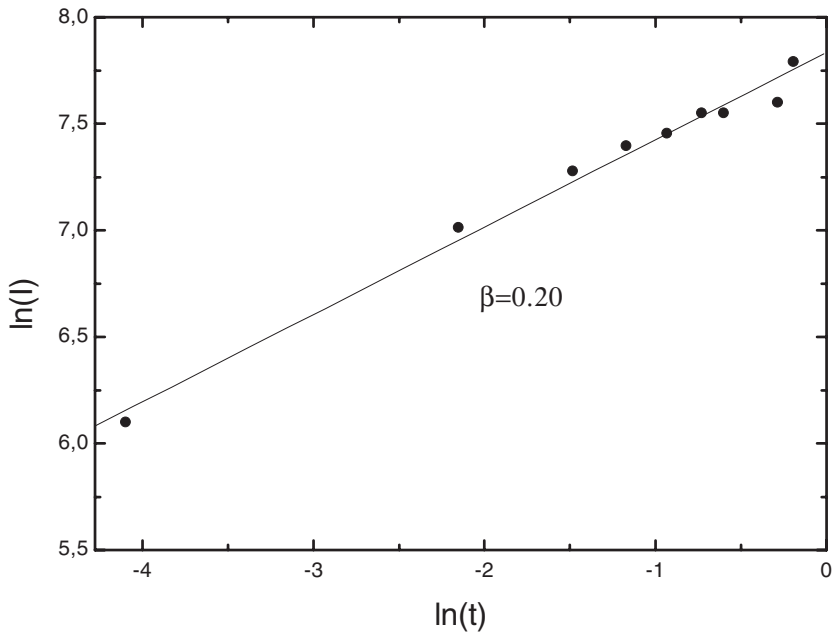

Figure 8. Logarithmic representation of Raman integrated intensity versus temperature for $K_{0.987}Cs_{0.013}MnF_3$ for the tetragonal mode located at 231.8 cm^{-1} at 140 K.

Acknowledgments

This work is a part of a co-operation between the University of Silesia and the Université du Maine; it was performed thanks to the financial support of the French Embassy in Warsaw, in the framework of a PhD fellowship. The authors would like to thank the cultural and scientific service of the Embassy for its support. We are also indebted to Professor M Rousseau for his invaluable discussions. The help of G Ripault in Raman-scattering technical assistance is also acknowledged.

References

[1] Beckman O and Knox K 1961 *Phys. Rev.* **121** 376
[2] Minkiewicz V J and Shirane G S 1967 *J. Phys. Soc. Japan* **26** 674
[3] Shirane G, Minkiewicz V and Linz A 1970 *Solid State Commun.* **8** 1941
[4] Lockwood D and Toriie B 1974 *J. Phys. C: Solid State Phys.* **7** 2729
[5] Hidaka M, Fuji H and Maeda S 1986 *Phase Transitions* **6** 101
[6] Gibaud A, Cowley R A and Nouet J 1989 *Phase Transitions* **14** 129
[7] Kapusta J, Daniel Ph and Ratuszna A 1999 *Phys. Rev.* B **59** 14 235
[8] Glazer A M 1972 *Acta Crystallogr.* B **28** 3384
[9] Gibaud A, Shapiro S M, Nouet J and You H 1991 *Phys. Rev.* B **44** 2437
[10] Ratuszna A and Kapusta J 1997 *Phase Transitions* **62** 181
[11] Skrzypek D, Jakubowski P, Ratuszna A and Chełłkowski A 1980 *J. Cryst. Growth.* **48** 475
[12] Rousseau D L, Baumann R P and Porto S P S 1981 *J. Raman Spectrosc.* **10** 253
[13] Barker A S Jr and Sievers A J 1975 *Rev. Mod. Phys.* **47** 1
[14] Chang I F and Mitra S S 1967 *Phys. Rev.* **172** 924
[15] Popkov Yu A, Eremenko V V and Fomin V I 1972 *Sov. Phys.–Solid State* **13** 1701
[16] Daniel Ph, Rousseau M, Désert A, Ratuszna A and Ganot F 1995 *Phys. Rev.* B **51** 12 337
[17] Di Antonio P, Vugmeister B E, Toulouse J and Boatner L A 1993 *Phys. Rev.* B **47** 5629

[18] Bruce A D, Taylor W and Murray A F 1980 *J. Phys. C: Solid State Phys.* **13** 483
[19] Daniel Ph, Rousseau M and Toulouse J 1997 *Phys. Rev.* B **55** 6222
[20] Kapusta J, Daniel Ph and Ratuszna A 2000 *Phase Transitions* **72** 165
[21] Ratuszna A, Daniel Ph, Kapusta J and Rousseau M 1998 *Phys. Rev.* B **57** 10 470
[22] Ratuszna A, Rybczyński J and Daniel Ph 1997 *Buletinul Stiintific al. Universitatii Politehnica* din Timisoara **42** 82
[23] Cowley R A 1980 *Adv. Phys.* **29** 1
Bruce A D 1980 *Adv. Phys.* **29** 111
Bruce A D and Cowley R A 1980 *Adv. Phys.* **29** 219
[24] Yacoby Y and Stern E A 1996 *Comments Condens. Matter Phys.* **18** 1